Over-wavelength pitch sized diffraction gratings for augmented reality applications

Valter Drazic, Oksana Shramkova, Bobin Varghese, Laurent Blondé, Vincent Brac de La Perrière, Jesse Schiffler, Patrice Twardowski, Sylvain Lecler, Benjamin Walter, Estelle Mairiaux, et al.

Research Article Vol. 30, No. 2 / 17 Jan 2022 / Optics Express 1293
Optics EXPRESS

Over-wavelength pitch sized diffraction gratings for augmented reality applications

VALTER DRAZIC,[1] OKSANA SHRAMKOVA,[1] BOBIN VARGHESE,[1] LAURENT BLONDÉ,[1] VINCENT BRAC DE LA PERRIÈRE,[1] JESSE SCHIFFLER,[1] PATRICE TWARDOWSKI,[2] SYLVAIN LECLER,[2] BENJAMIN WALTER,[2] ESTELLE MAIRIAUX,[3] FUANKI BAVEDILA,[3] MARC FAUCHER,[3,4] AND VALÉRIE ALLIÉ[3,4,*]

[1]*Interdigital R&D France, 975 avenue des Champs blancs, 35510 Cesson-Sévigné, France*
[2]*ICube Lab, Université de Strasbourg, CNRS, INSA Strasbourg . bld S. Brant, 67412 Illkirch, France*
[3]*Vmicro, bât. IEMN – Avenue Poincaré, 59650 Villeneuve d'Ascq, France*
[4]*Univ. Lille, CNRS, Centrale Lille, Univ.Polytechnique Hauts de France, UMR 8520 IEMN, Institut d'Electronique de Microélectronique et de Nanotechnologie, F 59000 Lille, France*
[*]*valerie.allie@interdigital.com*

Abstract: Waveguide based optical combiners for augmented reality (AR) glasses are integrating several surface relief gratings (SRG) whose pitch sizes can be as small as 200 nm for the blue wavelength. All SRG components exploit the first diffraction order to couple in and out or to deviate the light. We present SRG using higher diffraction orders featuring over-wavelength pitch sizes. Our gratings use the edge wave (EW) diffraction phenomenon to steer light in the preferred far field direction.

1. Introduction

One of the most challenging enablers for core AR technology is the combiner, which is the optical subset of the Head Mounted display (HMD) and smart glasses. It not only needs to be light, compact, exhibit a sufficient light efficiency and high transmittance for the real-world image, but also needs to accommodate requirements that are contradictory with the aforementioned ones: it needs to provide a very large Field Of View (FOV), a comfortable eye-box with a good spatial and angular uniformity [1–4]. The optical waveguide-based combiner is the most promising technology as it provides an eyeglass-like form factor together with a large eye-box [5]. The virtual image is generated by a light-engine which comprises a display, an illumination, and an imaging optical system. In case of virtual images displayed at large distances, the imaging optics has the function of a collimator. The exit pupil of the imaging optics is projected onto an input-coupler which is the entry port of the waveguide. The waveguides are divided as geometrical type [6] and diffractive type [7]. Geometrical waveguides use reflective and refractive optics to couple and de-couple light in and out of the waveguide. The main issues of geometrical systems are a small FOV and small eye-boxes. Diffractive waveguides employ diffraction gratings with four main technologies for in- and out-coupling: Surface Relief Gratings (SRGs) [8], Resonant Waveguide-mode Gratings (RWGs) [9] Volume Holograms (VH) [10] and metasurfaces [11]. SRGs and VHs will probably be the main competing technologies in the foreseeable future and could share a big part of HMDs market. The key parameters where both excel are the FOV and the illuminance uniformity [12]. The FOV is the angular range of the virtual image seen by the user. Illuminance uniformity characterizes two different aspects. First one is the spatial uniformity over the expanded exit-pupil, and the second one is the angular uniformity over the FOV. The combiner can be optimized as a system to exhibit a uniform image, but we can also optimize, as a pre-requisite, each building block individually. The building

#446077 https://doi.org/10.1364/OE.446077
Journal © 2022 Received 15 Oct 2021; revised 10 Dec 2021; accepted 16 Dec 2021; published 4 Jan 2022

Optics EXPRESS

blocks are the input-coupler, the Eye Pupil Expander (EPE) and the output-coupler. If their individual angular diffraction efficiency is high and uniform, then it is a good starting point for the combiner optimization process which proves otherwise to necessitate too many compromises to lead to efficient combiners. The waveguide's FOV is limited by the angular space between the critical and grazing angles inside of the waveguide for the image to be transported by Total Internal Reflection (TIR). One way to expand the FOV is to use symmetric input gratings to use two different propagation directions in the waveguide. Such a symmetric grating is tiling the exit pupil of the light engine in angular domain. Drazic et al. discuss the tiling of the exit pupil to expand the FOV above the state of the art for a multi-wavelength combiner system by multiplexing different solid angles of the light engine into the same or adjacent solid angles in the waveguide [13]. They also presented SRG optimized to use the second order diffraction in waveguide-based combiners [14]. The basic pattern of a symmetric-type input coupler was presented which had a high diffraction efficiency and uniformity. The advantage of using the second order diffraction is that the light gets more deviated than the first order, hence it is possible to work with higher pitch sizes for the grating to get the appropriate deviation needed to in-couple the image into the waveguide. Beginning with the description of the Edge Wave (EW) phenomenon in the next section, we want to present the basic ideas used to foster grating performances. In the third section, we describe an optimized input coupler, with calculated diffraction efficiencies. The fourth section describes the fabrication steps of a prototype and will present some electron-beam images and microscopic images of the grating. The final section will present the results of the measurements of the prototype and discuss them in relation to the simulations.

2. Edge wave enhanced surface relief gratings

SRG used as diffraction gratings for waveguide combiners have wavelength-scaled geometries consisting in straight edges. Under certain conditions on the refractive indexes, straight step dielectric edges illuminated by a plane wave are known to generate a near-field related dense photonic nanojet [15,16]. On the other hand, the different diffraction orders generated by SRG are a far field phenomenon. To enhance one of them, it is possible to take advantage of the Edge Wave (EW), which is a wave propagating into the far field, and which is a diffraction effect generated by straight steps [17]. The interference between the EW and the illuminating plane wave generates the nanojet in the near field. The EW propagation direction (Fig. 1) can be determined using the approximate formula:

$$\Theta_{EW1,EW2} \approx 90^\circ - \theta_{TIR} \pm \alpha \tag{1}$$

where Θ_{TIR} is the critical angle, α is the incident angle.

The typical structure that will be used in our gratings is a U-shaped geometry illustrated in Fig. 1.

Due to the proper combination of diffractive grating material n_2 with respect to surrounding media n_1, and material of the substrate n_3, with $n_3 > n_1$, the EWs are coupled into the waveguide. The complimentary input of the EWs into the light diffracted by the grating contributes to the formation of the final wavefront. The efficiency of some diffracted rays can be increased thanks to constructive interference of the diffracted light with the EWs of proper phase and direction.

A linear 1D diffraction grating made from U-shaped cells achieves symmetrical optical power distribution between diffraction orders ($T_j = T_{-j}$, $R_j = R_{-j}$, ..., where j is the diffraction order, T and R are the transmissivity and reflectivity of the gratings) leading to maximal grating efficiency for one couple of orders j. The periods of our diffraction gratings are defined to in-couple second diffraction order in the waveguides and the geometry of the U-shape optimized to get the highest possible diffraction efficiency and uniformity for that order.

To calculate the grating pitch, we assume that the biggest angular span that can be coupled propagates into the waveguide by TIR. A linearly polarized plane wave is incident on the

Optics EXPRESS

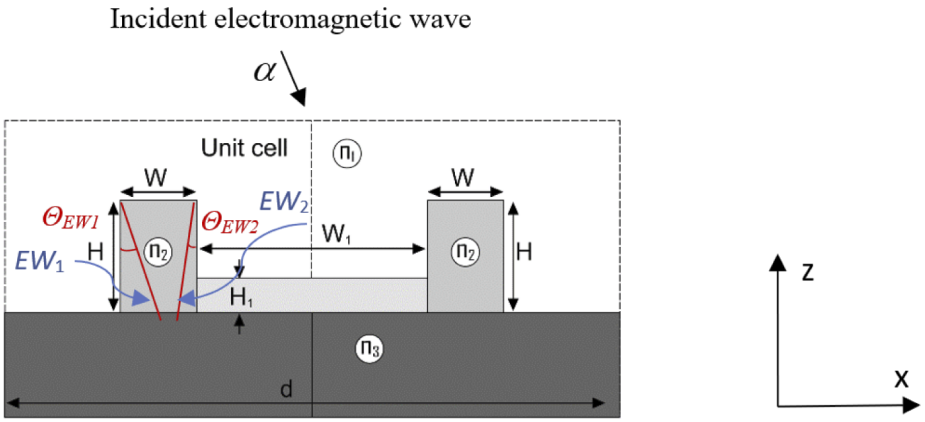

Fig. 1. Edge Waves generated by one of the pillars of the diffracting structure. Changing the sizes W, H of the pillars and W_1, H_1 of the bridge parts, we can modify the direction of the generated EWs. Above some angle of incidence a the right hand side pillar surface is reflecting the interior Edge Wave EW1.

gratings from the top. We must note that the proposed solution applies for TE (S) and TM (P) polarizations. However, to get the maximal efficiency, the system should be optimized considering the polarization of the incident wave.

Our input-coupler grating is designed to engage dual diffraction modes at each position for a large FOV and angular pupil tiling. In a dual-mode design, the + j^{th} order carries one half of the virtual image in one direction while the -j^{th} order does it for the other half in the opposite direction in the waveguide as shown in Fig. 2: rays incident on the in-coupler with angles $\pm\theta_1^C$ get diffracted inside the waveguide with angle $\pm\Phi_1^C$, while those with angles $\pm\theta_1^G$ get diffracted with angles $\pm\Phi_1^G$, respectively. This means that all rays on the right-hand side of $+\theta_1^G$ get diffracted into the waveguide and propagate to the right-hand side and those on the left-hand side of $-\theta_1^G$ get diffracted into the waveguide and propagate toward the left-hand side. Both halves of the virtual image are combined by the pupil expanders and out-couplers later inside the waveguide itself and the user sees one single virtual image. As depicted in Fig. 3, in-coupled light will be horizontally expanded by the two pupil expander gratings. Considering proper grating orientation, light will be diffracted towards a final grating ensuring vertical pupil expansion and out-coupling feature.

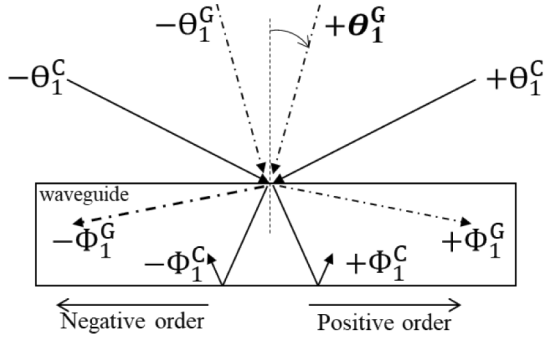

Fig. 2. Schematic of dual-mode pupil tiling diffraction grating design.

Optics EXPRESS

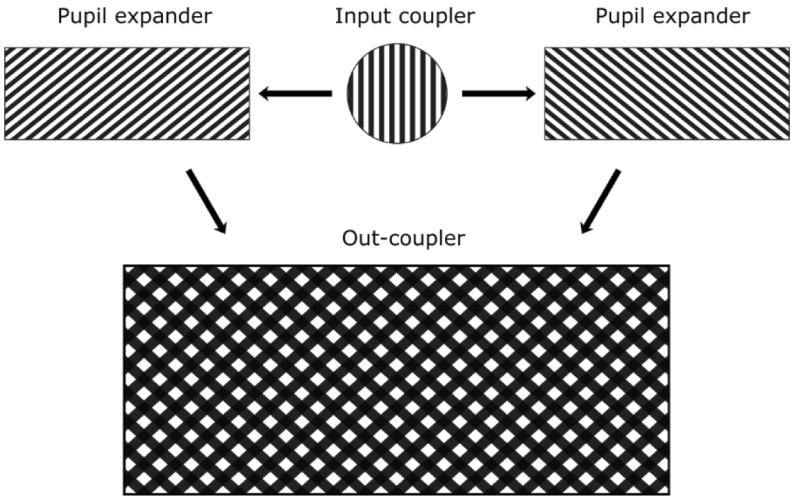

Fig. 3. Schematic of combiner with dual mode in-coupler, pupil expanders and out-coupler.

We determine the grating period keeping in mind the overlap required for conical illumination as well using the following relation:

$$\Lambda = m\frac{\lambda_0}{n_3 \sin \Phi_1^G + n_1 \sin \Theta_1^G} \tag{2}$$

where n_3 is the refractive index of the waveguide, n_1 the index of the surrounding media, m is the diffraction order (here $m = 2$), λ_0 is the free space wavelength (625 nm) and Λ is the grating period. Φ_1^G is the diffracted grazing angle and Θ_1^G will be set approximately equal to 3° to tile the pupil in two disjoint halves for the in-plane angles of incidence. Φ_1^G can have a maximum value of 90° which would be grazing to the surface of the waveguide and would not be useful for the subsequent elements in the waveguide. For this reason, we fix $\Phi_1^G = 75°$ in our work. As the waveguide used is a B270 glass of index $n_3 = 1.52$ for the design wavelength, the pitch size of the grating is $\Lambda = 822.4$ nm. The horizontal FOV for this system is set by the span $2\theta_1^C$ of the two outer angles that diffract just at the critical angles ${\Phi_1}^C$ in the waveguide, and it equals 56°.

3. Second order diffraction efficiency

Having the possibility to steer EW diffracted components into the direction of the second orders, we have a starting point to optimize the SRG under the finite element software Comsol Multiphysics. The U-shape index of refraction has been chosen as $n_2 = 2.105$ at the design wavelength because it is the index of the silicon nitride material of the prototype. We optimize W_1, W, H_1 and H in order to get the highest possible diffraction efficiency. Figure 4 shows various diffraction efficiency curves for the transmitted orders. The black curve illustrates the ±2 orders and achieves near to 75% value in the vicinity of ±28° angles of incidence. We have also plotted the transmitted ±1 and 0 orders. The sum of all transmitted light power is shown as the grey curve. The difference between the grey sum curve and the 100% level consists in the ±1 reflected orders. We see that the optimized ±2 order curves have a dip at normal incidence. This is only a pitch size issue. If we allow the overlap angle θ_1^G to take negative values instead of the chosen +3° one, that gap will be filled by a mix of the +2 and -2 orders, which means that around the normal, one part of the energy for a particular angle would diffract into the positive direction, while the complementary part will diffract into the negative direction. For the case of

Optics EXPRESS

overlapping some areas in the vicinity of the normal, more details can be found in [10], which details carefully how the overlap region is controlled.

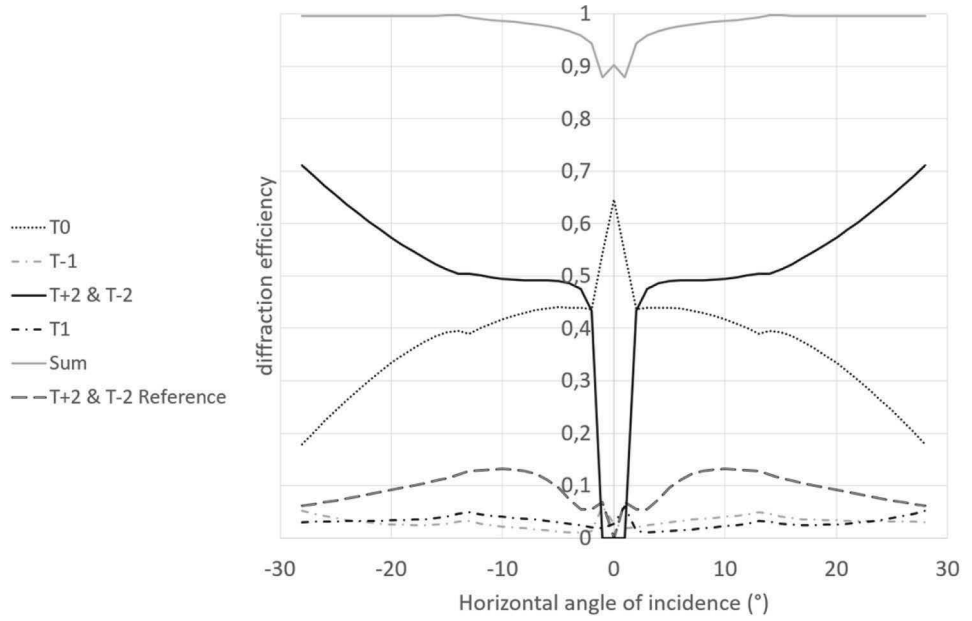

Fig. 4. Diffraction efficiency curves of a U-shaped periodic diffraction grating with the following parameters: n2 = 2.105, $\Lambda = 823$ nm, $W_1 = 260$ nm, $W = 120$ nm, $H_1 = 50$ nm, $H = 225$ nm.

We can also see in Fig. 4, that apart from the missing dip near normal incidence, the diffraction uniformity is very high. The diffraction uniformity is the ability of the system to maintain very high diffraction efficiencies over a large angular span. Here, in the ranges [-28°,-3] and [+3°,+28°], we have values of efficiency ranging from 45% to 71% approximately. Concerning the dimensions of the structure, the height is relatively shallow (below 250 nm), the width of the two pillars is compatible with Electron Beam Lithography (EBL) process. (120 nm). This patterning technology is an appropriate choice for prototyping or producing a small number of devices. To go into larger scale fabrication, optical lithography with high resolution steppers could be envisaged, benefiting from advanced techniques at 193nm [18] or from extreme-UV tools [19].

All dimensions have a tolerance of ±5 nm in order to maintain the desired diffraction efficiencies of ±2 orders.

Figure 4 shows also a 2nd order diffractive efficiency curves for a reference diffraction grating to benchmark the EW enhanced one with a state-of-the-art grating. The reference grating from Fig. 4 is a rectangular geometry (single block element with refractive index n2) of the same size than the U-shape one, same height and total width and the same grating period. We can see that the maximal efficiency of the second orders is below 15%.

To explain the effect of the EW and element's shape on the transmittivity of different orders, we analyze the E-field radiation pattern in the Far-Field (FF) for the U-shaped elements with refractive index $n_2 = 2.105$ surrounded by air. In Figs. 5(a) and (b) we can observe the nonsymmetric FF profiles of the electric field radiation with a strong principal lobe oriented along the angle of incidence and two less intensive side lobes. Analyzing the transmittivity for the periodic array of U-shaped elements, we can conclude that to improve the transmittivity of second order we

Optics EXPRESS

must align the deviation angles of secondary lobes with the second order deviation angle. A strategy for grating efficiency is combining cells, defining the grating pitch so that the second order is aligned with the lobe maximum and simultaneously the first order is in a low energy field radiation direction.

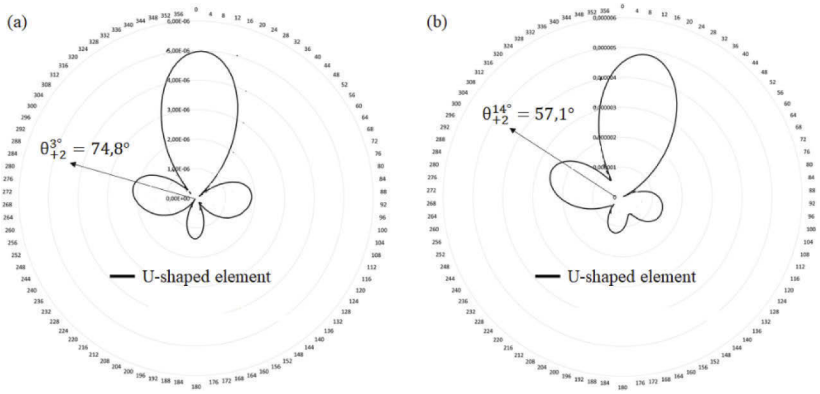

Fig. 5. Far field radiation pattern for the U-shaped geometry for 3°(a) and 14°(b) incident angles.

4. Fabrication process and sample structural measurements

The protypes are realized on B 270 i glass substrate from SCHOTT company. The substrates are 75mm x 75mm square shaped and 2.3 mm thick. A simplified process flow is presented on

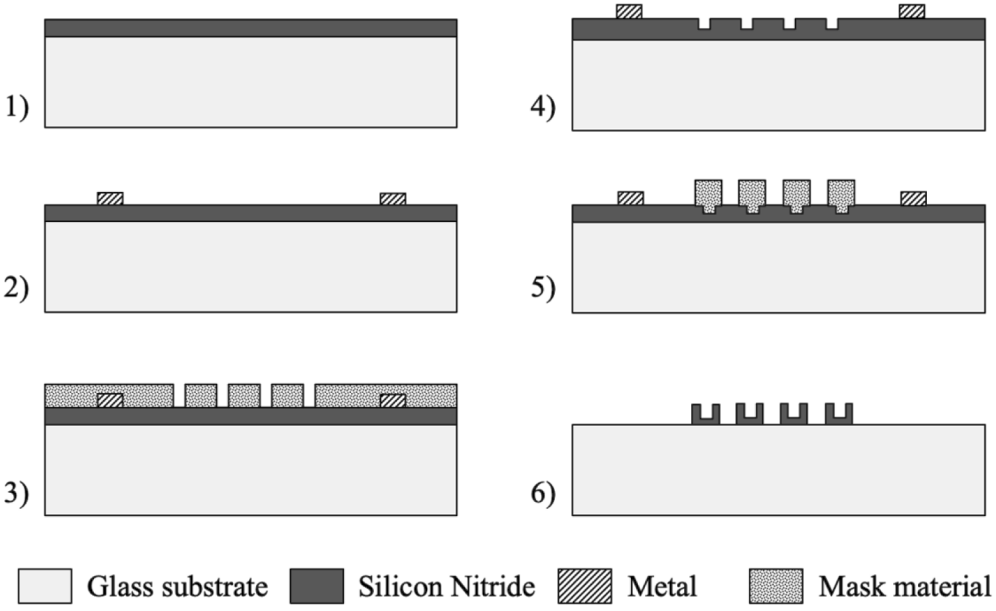

Fig. 6. Microfabrication process flow. 1) SiN deposited on top of a glass substrate. 2) alignment marks for e-beam lithography 3) e-beam lithography: mask open before the first etching step. 4) SiN partially etched. 5) e-beam lithography: grating definition. 6) final result after complete etching of the SiN layer.

Optics EXPRESS

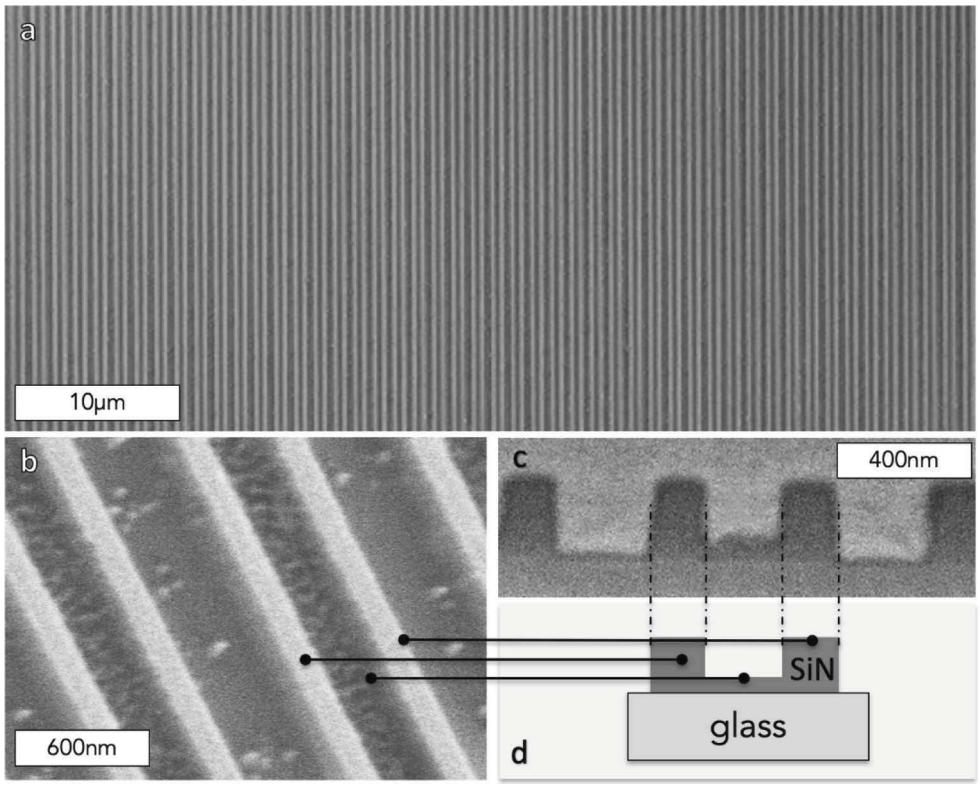

Fig. 7. a-b-c: SEM (Scanning Electron Microscope) picture of the grating, a: large view, b: tilted zoom, c: cross section by FIB (Focused Ion Beam). d: Schematic of one U-shaped unit.

Fig. 6. The first step is to deposit the grating material of index n_2. We select silicon nitride (SiN) as the grating material because (1-) it is an available material that is validated in cleanroom facilities, (2-) the index can be targeted precisely by tuning the deposition process parameters, (3-) the film thickness process precision fit the simulation needs (+/- 5 nm). The glass substrate transformation temperature T_g is 536°C. Thus, it can withstand a Plasma Enhanced Chemical Vapor Deposition technique at 300°C for silicon nitride deposition. By tuning the precursor gas ratio NH_3/SiH_4, the index varies from 2.02 to 2.3. The deposited silicon nitride layer index is measured at 2.108 and the thickness at 226nm, both by ellipsometry (Horiba UVISEL). The RMS Roughness (R_q) measured by Atomic Force Microscopy (AFM – Bruker Dimension Edge) is 0.31 nm.

The second step consists of pattering alignment marks for all subsequent EBL steps.

The third step aims at defining the interior of the U-shaped structures. To do so, we make an e-beam lithography with optimized alignment, which defines the mask material that will protect all the other areas. Then the SiN is partially etched in a RIE plasma. This requires a calibration to stop the etching at a given time.

At step 4, the mask material is chemically removed, and the surface is prepared for step 5. Here, an e-beam lithography followed by a plasma etching step are used to define the full U-shape. The same RIE process is applied to remove the SiN in both between the grating nanowires and outside of the grating area. For this prototype, the total grating surface is 2×2mm square, centered on the glass plate.

Optics EXPRESS

In Fig. 7, we present the fabricated prototype. Figure 7(a) is a large view of the grating and Fig. 7(b) is a tilted zoomed view. In this image we observe an apparent roughness in the middle of the U-shape structure which is due to partial etching of the SiN. Outside of the U-shape there are also small defaults. The etch rate of both SiN and glass (SiO_2) in RIE plasma etching is comparable, leading to a low selectivity between the targeted etched layer and the substrate. One must find a compromise between under-etching the SiN (and risk leaving a thin layer above the glass substrate) and over-etching it (leading to etching of the glass substrate as well). Regarding the targeted application, it was more important to preserve the glass substrate than to remove all the SiN particles. In a future realization, we propose to use a stop layer between the glass substrate and the SiN layer to be able to exactly etch the SiN layer without attacking the substrate. The index and thickness of such stopping layer should be taken into account in the optical simulations. Figure 7(c) is a cross-sectional image realized by FIB (Focused Ion Beam) to analyze the shape of the grating and the glass substrate etching. Since both the substate and the grating materials are dielectric, to obtain a better contrast, we deposited 10nm of carbon on top of the prototype before the FIB etching. This layer can be seen on the image between the U-shape as a dark layer. The substrate etching was measured below 10nm.

5. Performance measurement of prototypes

In order to measure the diffraction efficiency of the guided modes, samples are placed on an experimental setup which consists of illuminating the grating with a monochromatic plane wave, 3 mm diameter beam from a 632.8 nm He-Ne laser. The guided orders are extracted thanks to two Littrow non-coated N-BK7 prisms (30°/60°/90°).

The bonding of the two prisms is achieved by UV-curing Norland NOA65 adhesive whose refractive index is close to that of the prism. Each prism is separated by 9 mm from the center of the grating. This distance has been calculated to optimize the extraction of the guided modes after the first total internal reflection over the visible spectrum.

Finally, we have carried out the measurements according to the protocol of the following specifications: a polarization TE (S) of the beam, a scan from -32/32° with a step of 1° on the angle of incidence of the beam.

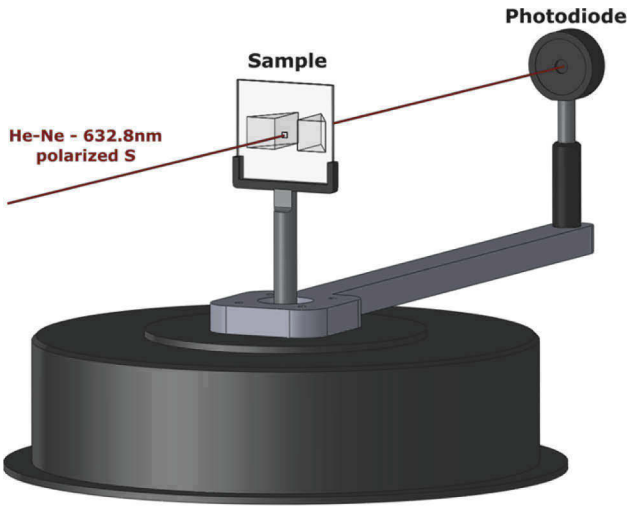

Fig. 8. Overview of the test bench (Transmitted Zero-order for a null incident angle)

Optics EXPRESS

The incident beam can be set by rotating the sample on the axis. The transmitted diffraction order powers are then measured with a photodiode, which can turn around the sample, as shown in the Fig. 8.

6. Comparisons with simulations and discussion

The measurements are compared with the simulations. As the gratings have symmetrical geometries, we will only show the results for negative angles of incidence even if we have measured the full range of in-plane incident angles and we have indeed a symmetry between positive and negative angles. In Fig. 9, the solid line represents the performances predicted in simulation for the specified grating. Once the grating was fabricated, we measured their geometry with an AFM. The geometry departed from the specified one and we did the simulation for that case, the results are shown in dotted line. Finally, the dashed line represents the measured diffraction efficiency. The Fresnel reflection coefficient from the extracting cube, which was not coated, has been taken into account and hence, the curve represents the in-coupling efficiency of the grating into the glass plate. Near normal incidence, it was expected that there is no in-coupled light, this is due to the grating pitch size, which was chosen to separate the negative and positive diffraction orders. At the value of 822 nm that we specified, there is a zone of ±3° near normal incidence where the diffraction efficiency is low. If the pitch size grows, that region shrinks. For angle of incidence below -3°, the diffraction efficiency raises almost continuously. In the simulation, at -30° the maximum diffraction efficiency was expected to be 60%. In the

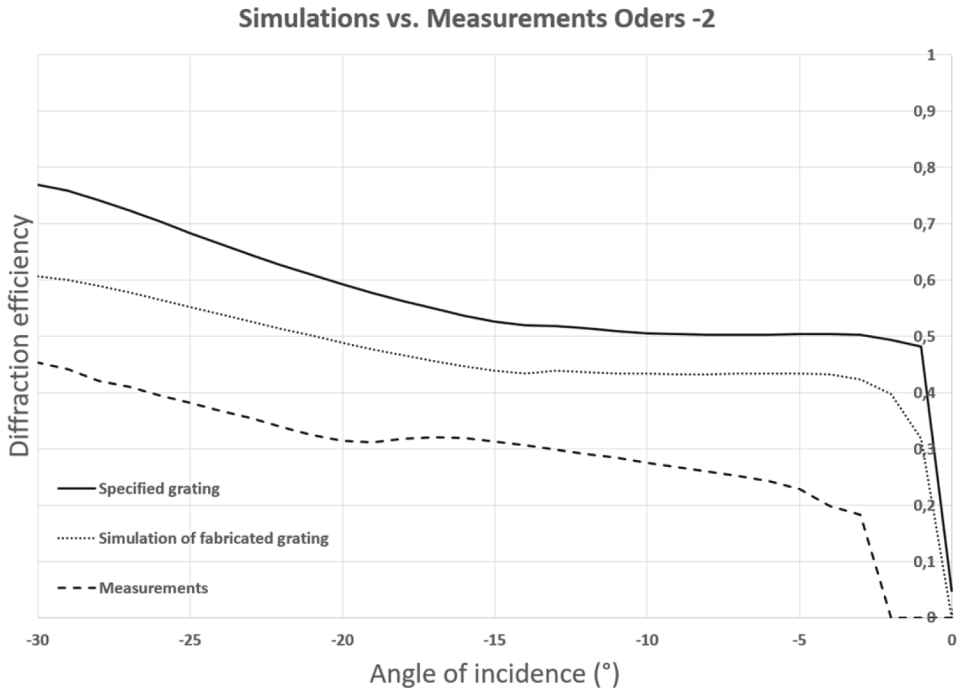

Fig. 9. Comparison of the simulations and measurements. The continuous line is the simulated diffraction efficiency with the optimal grating sizes of $\Lambda = 823$ nm, $W_1 = 260$ nm, $W = 120$ nm, $H_1 = 50$ nm, $H = 225$ nm. The dotted line curve shows the expected diffraction efficiency for the fabricated sample whose dimensions are $\Lambda = 829.5$ nm, $W_1 = 233.3$ nm, $W = 132.3$ nm, $H_1 = 90$ nm, $H = 229$ nm. The dashed line curve represents the measurements.

Optics EXPRESS

measurements, it is of 45%. We should remind here that we are measuring the second diffraction order, and not the first one. Generally, the second order carries much less power than the first order. This is a proof that our EW designed gratings reinforces the direction of the second order. But we can also design the geometry to emphasize even higher orders effectively. In that figure, we can also see that the global behavior of the measurements is varying as expected by the theory. The maximum diffraction efficiency is 30% below expectations. The measured efficiency is lower than expected and we tried to find out where this difference is going and why. For that purpose, we measured the other orders and found out that the transmitted order (zero order) is higher than expected. The transmitted zero order can only be measured between ±12° of incident angle approximately, because it hits the tips of the extracting prisms if the angles of incidence are out of this range. For the sample whose performances are reported in Fig. 9, at the angle of -10° for instance, the simulation is showing a diffraction efficiency of 34% for the order zero, while we measured an efficiency of 63%. At that same angle of incidence, the second order has a measured efficiency of 27.5% instead of an expected value of 43%.

The suspected reasons for the differences between the simulation and measurement are the fidelity of the shape of the grating to the specifications and the residual roughnesses. Indeed, a look at Fig. 7(c) shows the different issues that can potentially impact the performances. First, all corners are somewhat rounded. Next, the bottom of the U-shape, between the two pillars is rough and its geometry, instead of being flat varies from place to place. In Fig. 7(b), we can also see that there is residual material left by the etching on the glass substrate. It is not clear so far how each of these, affect the performances of the second order, therefore we propose some future fabrication process and design adaptation to improve global performances

7. Outlook

In this work we have demonstrated the validity of our EW based diffraction grating design and associated simulation thanks to a prototyping phase. Dual second order diffraction mode efficiency and uniformity has been measured. This phase has also demonstrated fabricability of the targeted SRGs and opens the way to future components evolutions

The problematic of the fabrication process is due to the fact that a glass substrate is used in a micro-fabrication facility mainly optimized to use semi-conductor materials. To get better geometries and validate our simulations with good measurements, it would be wishful to use a substrate compatible with the facilities processes. Secondly, the lithography of the geometry should use low absorbing silicon materials also showing a better compatibility with the processes.

On the optical design side, we also know that designing highly efficient in-couplers has also a downside. If the in-coupler is very efficient to deviate light into the waveguide, it is also very efficient to diffract light out of the waveguide, a phenomenon which is known as ‘back illumination’. Light in-coupled into the waveguide leaks out through the same in-coupler after the first total internal reflection in the waveguide. For a thinner waveguide, we would have more back reflections, and hence the very efficient in-coupler would be useless as it would also allow too much light to escape the waveguide. We have designed the previous prototype with a thickness of 2.3mm to avoid any back illumination of the in-coupler and measure its raw diffraction efficiency. But there are some future enhancements around to reduce the effect of the back illuminations while reducing the thickness of the waveguide. Among the ideas, which are not the primary topic of this publication, there are some optimized retarders that can be used to flip the polarization of the in-coupled light and lock it inside of the waveguide. This will be the focus of another communication.

Acknowledgments. This work is partly supported by the French RENATECH network.

Disclosures. VD, OS, BV, LB, VB, VA : InterDigital R&D France (E, P) - BW, EM, FB, MF : VMicro (E)

Optics EXPRESS

Data availability. Data underlying the results presented in this paper are not publicly available. They may be obtained from the authors upon reasonable request and provided an NDA is executed between the parties.

References

1. B. Kress, "Digital optical elements and technologies: applications to AR/VR/MR," Proc. SPIE **11062**, 1–13 (2019).
2. B. Kress and I. Chatterjee, "Waveguide combiners for mixed reality headsets: a nanophotonics design perspective," Nanophotonics **10**(1), 41–74 (2020).
3. T. Zhan, K. Yin, J. Xiong, Z. He, and S.-T. Wu, "Augmented Reality and Virtual Reality Displays: Perspectives and Challenges," iScience. **23**(8), 101397 (2020).
4. K. Yin, Z. He, J. Xiong, J. Zou, K. Li, and S.-T. Wu, "Virtual reality and augmented reality displays: advances and future perspectives," J. Phys. Photonics **3**(2), 022010 (2021).
5. R. Shechter, Y. Amitai, and A. A. Friesem, "Compact beam expander with linear gratings," Appl. Opt. **41**(7), 1236–1240 (2002).
6. D. Cheng, Y. Wang, C. Xu, W. Song, and G. Jin, "Design of an ultra-thin near-eye display with geometrical waveguide and freeform optics," Opt. Express **22**(17), 20705–20719 (2014).
7. J.-A. Piao, G. Li, M.-L. Piao, and N. Kim, "Full color holographic optical element fabrication for waveguide-type head mounted display using photopolymer," J. Opt. Soc. Korea **17**(3), 242–248 (2013).
8. T. Levola and P. Laakkonen, "Replicated slanted gratings with a high refractive index material for in and outcoupling of light," Opt. Express **15**(5), 2067–2074 (2007).
9. G. Basset, "Resonant screens focus on the optics of AR (Conference Presentation)," *Proc. SPIE 10676, Digital Optics for Immersive Displays*, 106760I (29 May 2018).
10. H. Mukawa, K. Akutsu, I. Matsumura, S. Nakano, T. Yoshida, M. Kuwahara, and K. Aiki, "A full-color eyewear display using planar waveguides with reflection volume holograms," J. Soc. Inf. Disp. **17**(3), 185–193 (2009).
11. F. Capasso, "The future and promise of flat optics: a personal perspective," Nanophotonics **7**(6), 953–957 (2018).
12. C. Pan, Z. Liu, Y. Pang, X. Zheng, H. Cai, Y. Zhang, and Z. Huang, "Design of a high-performance in-coupling grating using differential evolution algorithm for waveguide display," Opt. Express **26**(20), 26646–26662 (2018).
13. V. Drazic, O. Shramkova, B. Varghese, L. Blondé, and V. Allié, "Edge wave enabled diffractive optical elements for Augmented Reality glasses," *Optical Architectures for Displays and Sensing in Augmented, Virtual, and Mixed Reality (AR, VR, MR)* II (Vo. 11765, p. 117650A). International Society for Optics and Photonics (2021).
14. O. Shramkova, V. Drazic, B. Varghese, L. Blondé, V. Brac De La Perriere, and V. Allié, "High-uniformity dielectric U-shaped surface relief grating coupler for AR headsets," *Proc. SPIE 11802, Nanoengineering: Fabrication, Properties, Optics, Thin Films, and Devices* XVIII, 118020D (1 August 2021).
15. S. Lecler, Y. Takakura, and P. Meyrueis, "Properties of a three-dimensional photonic jet," Opt. Lett. **30**(19), 2641–2643 (2005).
16. A. Boriskin, V. Drazic, R. Keating, M. Damghanian, O. Shramkova, and L. Blondé, "Near field focusing by edge diffraction," Opt. Lett. **43**(16), 4053–4056 (2018).
17. B. Varghese, O. Shramkova, P. Minard, L. Blondé, V. Drazic, and V. Allié, "Experimental observation of asymmetrical microwave jets and far-field distribution generated by a dual-material system," Sci. Rep. **11**, 11871 (2021).
18. A. Raley, S. Thibaut, K. Subhadeep, N. Mohanty, R. Farrell, J. Smith, A. Metz, A. Ko, A. DeVillier, and P. Biolsi, "Novel patterning schemes and technologies for the sub 5 nm era," in *2018 International Symposium on VLSI Technology, Systems and Application (VLSI-TSA)*, 16-19 April 2018 2018, pp. 1–2.
19. A. Yen, H. Meiling, and J. Benschop, "Enabling manufacturing of sub-10 nm generations of integrated circuits with EUV lithography," in *2019 Electron Devices Technology and Manufacturing Conference (EDTM)*, 12-15 March 2019 2019, pp. 475–477.